0026-895X/05/6704-1067–1077$20.00
MOLECULAR PHARMACOLOGY
Vol. 67, No. 4
4713/1197421

Mol Pharmacol 67:1067–1077, 2005
Printed in U.S.A.

Molecular Determinants of Substrate/Inhibitor Binding to the Human and Rabbit Renal Organic Cation Transporters hOCT2 and rbOCT2

Wendy M. Suhre, Sean Ekins,[1] Cheng Chang, Peter W. Swaan, and Stephen H. Wright

Department of Physiology, University of Arizona, Tucson, Arizona (W.M.S., S.H.W.); Concurrent Pharmaceuticals, Ft. Washington, Pennsylvania (S.E.); and Department of Pharmaceutical Sciences, University of Maryland at Baltimore, Baltimore, Maryland (C.C., P.W.S.)

Received July 8, 2004; accepted January 3, 2005

ABSTRACT

Organic cation transporters are important for the elimination of many drugs and toxins from the body. In the present study, substrate-transporter interactions were investigated in Chinese hamster ovary cells stably transfected with either the human or rabbit orthologs of the principal organic cation transporter in the kidney, OCT2. IC_{50} values, ranging from 0.04 μM to >3 mM, for inhibition of [^{14}C]tetraethylammonium transport were determined for more than 30 structurally diverse compounds. Although the two OCT orthologs displayed similar IC_{50} values for some of these compounds, the majority varied by as much as 20-fold. Marked differences in substrate affinity were also noted when comparing hOCT2 to the closely related homolog hOCT1. These data suggest the molecular determinants of substrate binding differ markedly among both homologous and orthologous OCT transporters. The software package Cerius^2 (Accelrys, San Diego, CA) was used to generate a descriptor-based, two-dimensional, quantitative structure-activity relationship (QSAR) to produce a model relating the affinity of hOCT2 to particular physicochemical features of substrate/inhibitor molecules (r^2 = 0.81). Comparative molecular field analysis (Tripos, St. Louis, MO) was used to generate three-dimensional QSARs describing the structural basis of substrate binding to hOCT2 and rbOCT2 (q^2 = 0.60 and 0.53, respectively, and each with r^2 = 0.97). The quality of the models was assessed by their ability to successfully predict the inhibition of a set of test compounds. The current models enabled prediction of OCT2 affinity and may prove useful in the prediction of unwanted drug interactions at the level of the renal secretory process.

The kidneys play a key role in the secretion and subsequent elimination of drugs, toxins, and other xenobiotics from the body (Koepsell et al., 2003; Jonker and Schinkel, 2004; Koepsell, 2004; Wright and Dantzler, 2004). Many of these compounds are organic cations in that they carry a net positive charge at physiological pH, including compounds from a broad array of chemical and clinical classes (e.g., antiarrhythmics, β-adrenoreceptor blocking agents, antihistamines, antivirals, and skeletal muscle-relaxing agents). Organic cations (and bases; collectively OCs) are actively secreted by the proximal tubule by means of a two-step process (Wright and Dantzler, 2004). The first step involves transport of OC from the blood, across the basolateral membrane, into the proximal tubule cell via electrogenic, facilitated diffusion. The second step seems to be dominated by an organic cation/proton (OC/H^+) exchanger located in the apical membrane that transports the OC out of proximal cells into the tubular filtrate. Several of the organic cation transporters (OCTs) thought to play a role in the transport of these compounds across the basolateral membrane have been cloned in recent years, including OCT1, OCT2, and OCT3 (Koepsell et al., 2003; Koepsell and Endou, 2004; Wright and Dantzler, 2004). OCT1 and OCT2 seem to play the predominant role in secretion of the so-called "type I" OCs (i.e., generally monovalent, hydrophilic, mol. wt. <400; Meijer et al., 1990) in rodent and rabbit proximal tubules (Karbach

This work was supported by National Institutes of Health grants DK58251 (to S.H.W.), DK061425 (to P.W.S.), ES04940, ES06694, and HL07249.
[1] Current address: GeneGo, St. Joseph, MI 49085.
Article, publication date, and citation information can be found at http://molpharm.aspetjournals.org.
doi:10.1124/mol.104.004713.

ABBREVIATIONS: OC, organic cation; OCT, organic cation transporter; TEA, tetraethylammonium; CHO, Chinese hamster ovary; 2D, two-dimensional; 3D, three-dimensional; QSAR; quantitative structure-activity relationship; MPP, 1-methyl-4-phenylpyridinium; hOCT, human organic cation transporter; rbOCT, rabbit organic cation transporter; NBD-TMA, [2-(4-nitro-2,1,3-benzoxadiazol-7-yl)aminoethyl]trimethylammonium; WB, Waymouth buffer; CoMFA, comparative molecular field analysis; PLS, partial least square; PRESS, predictive error sum of squares; SNP, single nucleotide polymorphism.

et al., 2000; van Montfoort et al., 2001; Kaewmokul et al., 2003; Zhang et al., 2003). Indeed, active secretion of the prototypic type I substrate, tetraethylammonium (TEA) is eliminated in the OCT1/2 null mouse (Jonker et al., 2003). In the human, however, comparatively low expression of the mRNAs for OCT1 and OCT3, relative to OCT2 (Motohashi et al., 2002), supports the conclusion that OCT2 is probably the principal basolateral route for OC uptake into human proximal tubule cells. An understanding of the physical and structural characteristics that influence the binding of substrates to OCT2 would therefore assist in the development of models of substrate interaction with OCT2. Such models offer the promise of predicting clinically deleterious drug interactions and aiding in the design of novel pharmacological agents alongside the widely described in vitro and in vivo models used for generating much of the data on these transporters (Jonker and Schinkel, 2004).

Previous studies have shown hydrophobicity and basicity to be important determinants of substrate specificity for OCTs in the apical and basolateral membranes of the rat proximal tubule (Ullrich et al., 1991; Ullrich, 1999). More recent work has shown that placement of planar hydrophobic mass, relative to a positively charged nitronium nucleus, is important for substrate binding to hOCT1 (Bednarczyk et al., 2003) and to the OC/H^+ exchanger in rabbit renal brush-border membrane vesicles (Wright and Wunz, 1999). In contrast, relatively little is known of the structural requirements for OCT2 substrate binding, other than the critical role of the degree of ionization identified by the increased IC_{50} values of weak bases when external pH is shifted from 7 to 8 (thereby decreasing protonation; Barendt and Wright, 2002). In the present study, substrate/transporter interactions were investigated on a much larger scale in an attempt to identify distinct molecular characteristics that play a role in selectivity of OCT2. To accomplish this, a set of structurally diverse compounds was chosen for inhibition studies with the human and rabbit orthologs of OCT2 that were stably transfected in Chinese hamster ovary (CHO) cells. This effort to develop a strategy for predicting molecular criteria that influence binding to OCT2 involved use of two different computational methods to generate 2D- and 3D-quantitative structure activity relationship (QSAR) models. Whereas both approaches proved more effective for predicting substrate-transporter interactions than simple substrate hydrophobicity, the 3D-QSAR proved to have greater predictive power, suggesting that steric factors play a more important role in the binding process than previously acknowledged.

Materials and Methods

Chemicals. [^{14}C]TEA (55.6 Ci/mmol) was acquired from Wizard Laboratories, Inc. (West Sacramento, CA). 1-Methyl-4-phenylpyridinium (MPP) was from Sigma/RBI (Natick, MA). 1,3,5-Trimethyl-4-phenylpyridinium, 2,4-dimethyl-9-*H*-indenol[2,1-*c*]pyridinium, and 3,5-dimethyl-4-phenylpyridinium oxide were synthesized by the Synthesis Core of the Southwest Environmental Health Sciences Center and the Department of Chemistry at the University of Arizona (Tucson, AZ). [2-(4-Nitro-2,1,3-benzoxadiazol-7-yl)aminoethyl]trimethylammonium (NBD-TMA) was synthesized as described previously (Bednarczyk et al., 2000). The set of N^1-substituted pyridiniums and quinoliniums and ethylacridinium were synthesized as described previously (Wright et al., 1995). All other chemicals were acquired from Sigma-Aldrich (St. Louis, MO) or other standard sources and were the highest grade available.

CHO Cell Culture and Stable Expression of hOCT2 and rbOCT2. CHO cells were acquired from the American Type Culture Collection (Manassas, VA) and grown in Ham's F-12 Kaighn's modification (Sigma-Aldrich) containing 10% fetal bovine serum (Hyclone Laboratories, Logan, UT) and maintained in a humidified atmosphere with 5% CO_2. For stable expression of hOCT2 and rbOCT2, cells were electroporated with 10 μg of pcDNA3.1 plasmid DNA containing the hOCT2 or rbOCT2 construct and 10 μg of salmon sperm (Invitrogen, Carlsbad, CA) in a cuvette (4-mm gap) using a BTX ECM 630 electroporator with settings of 1050 μF, 260 V, and no resistance. Forty-eight hours after the electroporation, positively transfected cells were identified (based upon their ability to accumulate the fluorescent OC NBD-TMA; Bednarczyk et al., 2000) and selected with 1 mg/ml Geneticin (Invitrogen). Clones that continued to accumulate NBD-TMA were tested for transport of [^{14}C]TEA, and the clones that displayed the highest rate of TEA uptake were characterized in greater detail. The time course and kinetics of TEA transport were measured in experiments using several successive passages of each cell line. Values for J_{max} and K_t for TEA transport were consistently similar for the individual clones of each transporter. Therefore, representative cells lines expressing either hOCT2 or rbOCT2 were selected to conduct the subsequent experiments in this study.

Transport Experiments. CHO^{hOCT2} and CHO^{rbOCT2} cells were seeded in 12-well plates (USA Scientific, Ocala, FL) and grown to confluence. Once confluent (typically 24–48 h), transport experiments were conducted by aspirating the media and preincubating each well of cells in two successive 15-min exposures to 1 ml of Waymouth buffer (WB) (135 mM NaCl, 13 mM HEPES, 2.5 mM $CaCl_2 \cdot 2H_2O$, 1.2 mM $MgCl_2$, 0.8 mM $MgSO_4 \cdot 7H_2O$, 5 mM KCl, and 28 mM glucose). After the preincubations, 400 μl of "transport buffer" containing (typically) 0.4 μCi/ml [^{14}C]TEA (~10 μM), and, in some cases, increasing concentrations of a test inhibitor in WB, were added to the wells. At intervals, the transport buffer was removed, and each well was rinsed three times with 2 ml of ice-cold WB containing 250 μM tetrapentylammonium to stop transport. Cells were solubilized with 400 μl of 0.5 N NaOH in 1% SDS by shaking for 30 min. Solubilized cells were neutralized with 200 μl of 1 N HCl, the solution was triturated, and 500 μl was removed and placed in a scintillation vial. The amount of radioactivity in each sample was determined using scintillation spectrometry (Beckman model LS3801). Individual transport observations were performed in triplicate for each experiment, and observations were confirmed, typically two or three times (i.e., $n = 2$ or 3), in separate experiments using different cell passages. All experiments were performed between passages 4 and 40 (postcloning), with no appreciable difference in the results obtained with early versus later passages (i.e., little change in K_t for TEA).

Modeling with Cerius^2. The computational molecular modeling studies were carried out as described in more detail previously (Bednarczyk et al., 2003) using a Silicon Graphics Octane workstation (SGI, Mountain View, CA). Molecular structures were used as either SMILES or sdf format and imported into Cerius^2 version 4.8 (Accelrys, San Diego, CA). Cerius^2 QSAR was used to generate 54 descriptors, including the default, Jurs descriptors, Shadow indices, and Octanol/water partition coefficients (ALogP98 and ClogP) for the molecules of the training and test sets. The forward stepwise regression method incorporated within Cerius^2 was then used to relate the log IC_{50} to a selection of these descriptors, and hence result in a QSAR model. The model was validated for numerical stability and internal consistency using both the Leave-One-Out cross-validation method and by permuting, or randomizing, the response variable a number of times.

Comparative Molecular Field Analysis. CoMFA attempts to explain the gradual changes in observed biological properties by evaluating the electrostatic (Coulombic interactions) and steric (van

der Waals interactions) fields at regularly spaced grid points surrounding a set of mutually aligned ligands. OCT2 substrates were assigned partial atomic (point) charges at neutral pH (7.4) by performing a 1SCF MOPAC calculation using the AM1 Hamiltonian (keywords EF, PRECISE, MMOK). Molecules containing positive ionizable groups with a $pK_a > 8.4$ (i.e., >90% ionized at pH 7.4) were modeled in the charged state using the additional keyword CHARGE = 1. Molecules were superimposed using the FieldFit routine in Sybyl and imported into a molecular spreadsheet. Partial least square (PLS) was used to correlate the field descriptors with biological activities. Both fields were calculated using an sp3 hybridized carbon probe atom (+1 charge at 1.52-Å van der Waals radius) on a 2.0-Å spaced lattice, which extends beyond the dimensions of each structure by 4.0 Å in all directions. A cut-off of 30 kcal/mol ensures that no extreme energy terms will distort the final model. The indicator fields and hydrogen bond fields generated by the "advanced CoMFA" module were also included in the analysis. To eliminate excessive noise, all electrostatic energies below 1.0 kcal/mol and steric energies below 10.0 kcal/ mol were set to zero. CoMFA descriptors were used as independent variables, whereas the dependent variable (biological descriptor) used in these studies was log IC_{50}. Experimental standard deviations were used as a weighting factor in PLS analyses. The predictive value of the models was evaluated first using Leave-One-Out cross-validation. The cross-validated standard coefficient, q^2, was calculated as follows:

$$q^2 = 1 - \frac{\sum_Y (Y_{\text{predicted}} - Y_{\text{observed}})^2}{\sum_Y (Y_{\text{observed}} - Y_{\text{mean}})^2} \quad (1)$$

where $Y_{\text{predicted}}$, Y_{observed}, and Y_{mean} are the predicted, observed, and mean values of the target property (IC_{50}), respectively. $\Sigma(Y_{\text{predicted}} - Y_{\text{observed}})^2$ is the predictive error sum of squares (PRESS). The standard error of the cross-validated predictions is represented as *press*, whereas the root mean squares of the conventional (non–cross-validated) analysis is known as (*s*). The model with the optimum number of PLS components, corresponding to the lowest PRESS value, was selected for deriving the final PLS regression models. In addition to the q^2, the conventional correlation coefficient, r^2, and its standard error were also calculated. A plot of predicted versus experimental activity was used to identify potential outliers. The process was repeated until no further improvements in q^2 or no outliers could be identified. Results from alternative descriptor fields were compared, and the model with the highest q^2 was accepted. A contour plot of standard coefficients enclosing the highest 20% value was created for each model.

HipHop Pharmacophore Development. Pharmacophore models were constructed using Catalyst version 4.9 (Accelrys) to generate a common features (HipHop) (Clement and Mehl, 2000) pharmacophore for the selective inhibitors of rbOCT2 (cimetidine, guanidine, NBD-TMA, N^1-hydroxyethylpyridinium) and hOCT2 (carbachol, tyramine, choline, nicotine, metformin, and serotonin). Tetrapropylammonium, clonidine, and tetrabutylammonium were comparatively selective inhibitors for rbOCT2 but were severely limited in the number of molecular features that could be used for successful pharmacophore generation and were therefore excluded from our analysis.

Up to 255 conformers were generated for each molecule with the fast conformer generation method, allowing a maximum energy of 20 kcal/mol. The principal molecule for hOCT2 was carbachol, to which the other molecules were aligned, whereas for rbOCT2 the molecules were aligned to cimetidine. Substrate molecules were then aligned using hydrophobic, hydrogen bond acceptor, hydrogen bond donor, and positive charge and positive ionizable features in the HipHop algorithm within Catalyst.

Results

Kinetics of TEA Transport Mediated by the Human and Rabbit Orthologs of OCT2. Fig. 1 shows the time course of [^{14}C]TEA transport into CHO cells that stably expressed either hOCT2 (Fig. 1A) or rbOCT2 (Fig. 1B). In both cases, accumulation of labeled substrate increased with time in a near linear manner for 5 min and was blocked ~95% by coexposure to 2.5 mM unlabeled TEA. Extrapolation of these time courses to time 0 resulted in positive intercepts. This did not represent nonspecific binding of labeled substrate to the cells or residual label left after rinsing, both of which would have been revealed in the level of activity measured in the presence of 2.5 mM unlabeled TEA. These positive intercepts were only noticed in cells that expressed transporter; accumulation of [^{14}C]TEA into wild-type CHO cells was the same low level as that noted in transporter-expressing cells when blocked by unlabeled TEA (data not shown). Busch et al. (1998) noted that uptake of MPP into human embryonic kidney-293 cells that stably expressed hOCT2 occurs very rapidly, reaching steady state within 5 to 10 s. However, in the present case, the "rapid" uptake of TEA into OCT2-expressing CHO cells did not represent an approach to steady state, but it was followed for many minutes by a continuous, time-dependent component of mediated transport. Whereas the mechanistic basis of the rapid component of [^{14}C]TEA accumulation is not known, it had kinetic properties effectively identical to the fraction of total uptake that clearly represented time-dependent cellular transport, as discussed below. Therefore, for the subsequent kinetic analyses, we used 5- or 2-min uptakes of [^{14}C]TEA to provide estimates of the initial rate of TEA uptake into CHO^{hOCT2} or CHO^{rbOCT2}, respectively.

Figure 2 shows the kinetics of TEA transport into CHO^{hOCT2} (Fig. 2A) or CHO^{rbOCT2} (Fig. 2B). For both processes, the addition of unlabeled TEA inhibited uptake of [^{14}C]TEA by a process adequately described by the Michaelis-Menten equation for competitive interaction of the labeled and unlabeled substrate (Malo and Berteloot, 1991):

$$J = \frac{J_{\max}[{}^*T]}{K_t + [{}^*T] + [T]} + C \quad (2)$$

where J is the rate of [^{14}C]TEA transport from a concentration of labeled substrate equal to [*T]; $J_{\max}$ is the maximum rate of mediated TEA transport; K_t is the TEA concentration

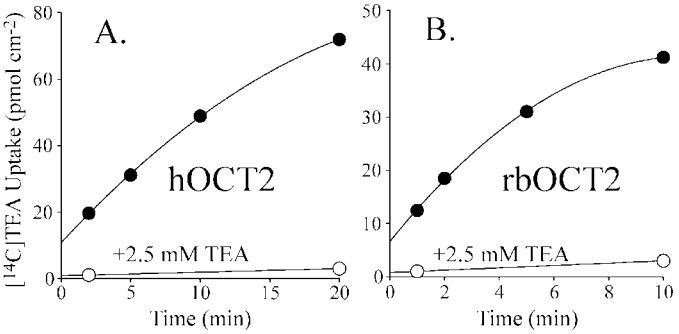

Fig. 1. Time course of TEA uptake into CHO cells stably transfected with either hOCT2 (A) or rbOCT2 (B). Each point is the mean (±S.E.) of triplicate measures of 16 μM [^{14}C]TEA uptake at each time point, determined in a single representative experiment. Uptake was measured in the absence and presence of 2.5 mM unlabeled TEA.

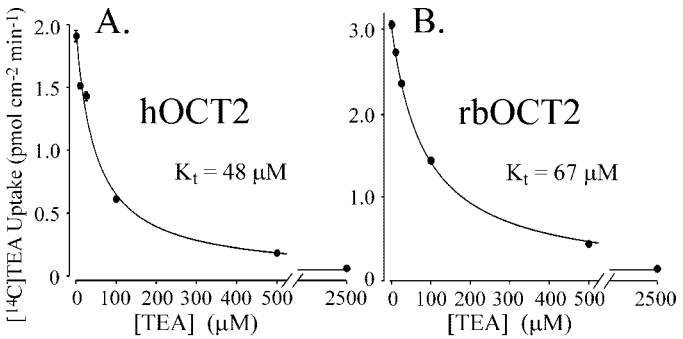

Fig. 2. Kinetics of TEA transport in CHO cells stably transfected with either hOCT2 (A) or rbOCT2 (B). Five-minute (hOCT2) or 2-min (rbOCT2) uptakes of 7.2 μM [^{14}C]TEA were measured in the presence of increasing concentrations of unlabeled TEA (0–2500 μM). Each data point is the mean (±S.E.) triplicate measures of uptake in a single experiment. For the representative experiments shown, the K_t and J_{max} for TEA uptake was, respectively 48 μM and 11.6 pmol cm^{-2} min^{-1} for hOCT2, and 67 μM and 14.4 pmol cm^{-2} min^{-1} for rbOCT2. Lines were fit to the data using a nonlinear regression algorithm (SigmaPlot 3.0).

that resulted in half-maximal transport (Michaelis constant); [T] is the concentration of unlabeled TEA in the transport reaction; and C is a constant representing the component of total TEA uptake that was not saturated (over the range of substrate concentrations tested) and presumably reflected the combined influence of diffusive flux, nonspecific binding, and/or incomplete rinsing of the cell layer. In three separate experiments, the K_t values for TEA transport mediated by hOCT2 or rbOCT2 were 47.2 ± 2.2 and 80.9 ± 13.3 μM, respectively (with J_{max} values of 8.0 ± 2.0 and 29.6 ± 18.9 pmol cm^{-2} min^{-1}, respectively). As alluded to earlier, analysis of the residuals determined from fitting eq. 1 (Malo and Berteloot, 1991) to the kinetic data suggested that the saturable component of TEA transport was adequately described by the activity of a single, hyperbolic process. The same observation was evident in the (upcoming) analyses of inhibitor interaction with these transporters. We interpreted this as indicating that the rapid, displaceable binding component of OC accumulation in these cells involved kinetics very similar to that of the time-dependent element of OC uptake, and, consequently, would have little effect on the calculation of the kinetic constants K_t, K_i, or IC_{50}.

Inhibition of OCT2 Activity by Selected Organic Electrolytes. In an attempt to develop a model of the physical and structural basis of substrate-transporter interaction for OCT2, we assessed the kinetics of inhibition of [^{14}C]TEA transport produced by an array of potential substrates for human and rabbit OCT2. With the exception of several anionic inhibitors, the kinetics of inhibition were well described by the following relationship (Groves et al., 1994):

$$J = \frac{J_{app}[T^*]}{K_{app} + [I]} + C \quad (3)$$

where J_{app} is defined as $(K_i/K_t)J_{max}$, [I] is the concentration of the test agent, and K_{app} is an apparent inhibitory constant (K_i) for the test agent that is defined as $K_i(1 + [T^*]/K_t)$. When [T^*] is $\ll K_t$, $K_{app} \approx K_i$. The application of this equation carries the tacit assumption that the inhibitory interactions observed are competitive in nature and reflect binding of substrate and inhibitor at a common binding site. Although that is demonstrably the case for certain compounds (e.g., cimetidine, tyramine, and NBD-TMA; Bednarczyk et al., 2000; Kaewmokul et al., 2003; our unpublished observations), and reasonably assumed to be the case for others (owing to marked structural similarities with molecules known to be OCT2 substrates), we have not rigorously proven this to be the case for all compounds used in this study. Therefore, we will henceforth refer to the kinetic constants calculated through application of eq. 2 as "IC_{50}" values.

The test agents used here were selected to represent a broad range of the parameters suspected of influencing binding to the transport site of OCT2, including hydrophobicity (e.g., ClogP and ALogP98), molecular weight, basicity, and 3D configuration. In addition, we considered it important to have compounds for which OCT2 displayed a broad range of apparent affinities to generate QSAR models. Figure 3 shows the effect of increasing the test agent concentration on the inhibition of TEA transport mediated by either hOCT2 (Fig. 3A) or rbOCT2 (Fig. 3B) for four representative compounds (ethylacridinium, clonidine, tyramine, and guanidine) with IC_{50} values that spanned 5 orders of magnitude. Table 1 lists the IC_{50} values for the compounds included in the training and test sets examined in this study. It is interesting that these orthologous transporters displayed both remarkable similarities in their apparent affinities for selected compounds, and marked differences. For example, whereas human and rabbit OCT2 had virtually identical IC_{50} values for ephedrine (Fig. 4A), hOCT2 had a 10-fold higher apparent affinity for carbachol (than rbOCT2; Fig. 4B), whereas rbOCT2 had a 20-fold higher apparent affinity for cimetidine (than hOCT2; Fig. 4C). Figure 5 compares the IC_{50} values measured for the battery of test agents against TEA transport mediated by hOCT2 (x-axis) and rbOCT2 (y-axis). Although it is evident that there was a marked correlation between increasing IC_{50} values measured for inhibition of hOCT2-mediated TEA transport and parallel increases mea-

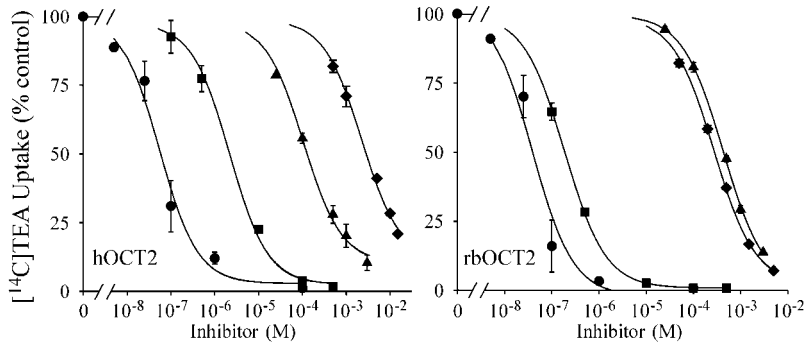

Fig. 3. Effect of increasing concentration of several test inhibitors on uptake of [^{14}C]TEA mediated by either hOCT2 (left) or rbOCT2 (right). Each point is the mean (±S.E.) of uptakes measured in two or three separate experiments with each test compound. IC_{50} values were (for hOCT2 and rbOCT2, respectively) as follows: ethylacridinium (●), 0.09 and 0.04 μM; clonidine (■), 2.2 and 0.19 μM; tyramine (▲), 106 and 426 μM; and guanidine (◆), 2300 and 272 μM.

sured for rbOCT2, on average, IC_{50} values measured for the rabbit ortholog were approximately 50% lower than those measured for the human ortholog. Nevertheless, as suggested by the data presented in Fig. 4, there were a number of exceptions to this general rule. Figure 6 shows the ratio of IC_{50} values measured for hOCT2- versus rbOCT2-mediated transport. Whereas the rabbit OCT2 ortholog displayed a significantly greater affinity (than the human) for nine of 28 compounds tested, eight of 28 compounds showed the opposite, i.e., hOCT2 displayed a greater affinity for them than did rbOCT2.

As previously mentioned, a positive correlation between hydrophobicity and affinity has been reported for the interaction of substrates and inhibitors of renal OC transporters (Ullrich et al., 1991). Figure 7 shows the relationship between IC_{50} and ALogP98 of the diverse group of inhibitors of hOCT2 used in the present study. Although there was a significant correlation between these parameters, it was comparatively modest ($r^2 = 0.38$) and numerous "outliers" were evident. It is also relevant to note that a plot of IC_{50} versus another commonly used calculated hydrophobicity indicator, ClogP, suggested that there was no significant correlation between these parameters (data not shown). This somewhat unexpected observation reflects the fact that the commonly used algorithms for calculation of octanol/water partition coefficients frequently show rather modest agreement with one another, as shown by the comparatively weak correlation ($r^2 = 0.27$) between ALogP98 and ClogP values for the compounds used in the present study (data not shown). We raise this issue because it underscores the desirability of developing a more precise means to predict the relationship between substrate structure and binding to OCT2 rather than using a predicted measure of hydrophobicity alone.

TABLE 1

Observed IC_{50} values for hOCT2 and rbOCT2 for structurally diverse organic cations

Each IC_{50} is the mean value of at least two separate experiments (described under *Materials and Methods*).

Compound	hOCT2 IC_{50}	rbOCT2 IC_{50}
	μM	
Training set		
Ethylacridinium	0.09 ± 0.03	0.04 ± 0
2,4-DIPyr	0.34 ± 0.20	0.40 ± 0.03
1,3,5-TPPyr	0.77 ± 0.07	0.61 ± 0.06
Clonidine	2.2 ± 0.51	0.19 ± 0.02
MPP	2.4 ± 0.04	1.4 ± 0.17
Crystal violet	2.6 ± 1.20	2.05 ± 0.15
Tetrapentylammonium	10.5 ± 3.09	10.4 ± 5.2
NBD-TMA	13.5 ± 2.50	2.3 ± 0
Phenformin	15.3 ± 1.86	7.3 ± 1.5
Tetrabutylammonium	19.5 ± 1.50	2.9 ± 0.26
Tetrapropylammonium	20.0 ± 0.58	1.6 ± 0.29
Nicotine	22.2 ± 3.05	55.2 ± 5.10
Ephedrine	29.0 ± 1.00	31.0 ± 3.00
Ranitidine	39.7 ± 16.10	27.0 ± 5.00
TEA	46.3 ± 1.89	86.5 ± 20.50
Pindolol	50.5 ± 3.50	67.5 ± 10.50
4-Phenylpyridine	57.5 ± 16.50	37.5 ± 3.50
Cimetidine	70 ± 10.00	3.3 ± 0.33
Tyramine	106 ± 2.0	426 ± 8.0
1-(2-Hydroxyethyl)pyridinium	112 ± 17.5	42.0 ± 3.00
Carbachol	248 ± 23.0	1439 ± 89
N^1-Methylnicotinamide	303 ± 15.4	180 ± 13.0
Serotonin	310 ± 18.0	664 ± 44
Metformin	339 ± 5.3	808 ± 94
Choline	381 ± 75.6	1388 ± 401
Tetramethylammonium	525 ± 109	850 ± 44
Guanidine	2300 ± 536	272 ± 16
Histamine	3251 ± 497	427 ± 135
Test set		
Cyclohexylamine	8.2 ± 0.80	18.0 ± 1.00
3,5-Dimethyl-4-phenylpyridine- 1-oxide	11.9 ± 3.15	47.0 ± 12.00
Amantadine	19.7 ± 3.56	31.7 ± 5.00
Procainamide	57.5 ± 1.50	30.0 ± 9.0
Famotidine	111 ± 38.0	7.4 ± 1.20
Ibuprofen	~10 mM	3100 ± 500

2,4-DIPyr, 2,4-dimethyl-9-*H*-indenol[2,1-*c*]pyridinium; 1,3,5-TPPyr, 1,3,5-trimethyl-4-phenyl pyridinium.

Generation of QSAR Models for hOCT2–2D-QSAR (Cerius^2). The comparatively weak correlation between substrate/inhibitor hydrophobicity and the measured interaction with hOCT2 led us to consider a more rigorous method for developing a predictive model of substrate-transporter binding. We have previously used Cerius^2 to develop a descriptor-based QSAR model of substrate binding to hOCT1 (Bednarczyk et al., 2003), an approach that proved to be superior to one based on the use of Catalyst to develop a 3D pharmacophore of binding to the transporter. Therefore, a descriptor-based 2D-QSAR model for hOCT2 was built using a small selection of the molecular descriptors generated by Cerius^2. The following equation, produced using forward stepwise regression, incorporates the five molecular descriptors of the training set of 30 molecules that proved to be most strongly correlated with inhibition of hOCT2 activity:

$$\text{Log } IC_{50} = -0.925378 + 0.125798 \times \text{Rotatable bonds} - 0.412128 \times \text{ALogP98} + 4.05786 \times \text{Jurs-RNCG} + 1.62335 \times \text{Jurs RPSA} + 0.02947 \times \text{Shadow YZ} \quad (4)$$

In this equation, RNCG represents the charge of the most negative compound divided by the total negative charge, RPSA is the relative polar surface area, and shadow YZ is the area of projection in the YZ plane. Figure 8A shows the correlation between the hOCT2 IC_{50} values measured using the CHO^{hOCT2} cells and those predicted by the Cerius^2 model; the model yielded an $r^2 = 0.92$, Leave-One-Out $q^2 = 0.74$, and F-test = 20.9 for the compounds comprising the training set. The model was randomized 9 times to give 90%

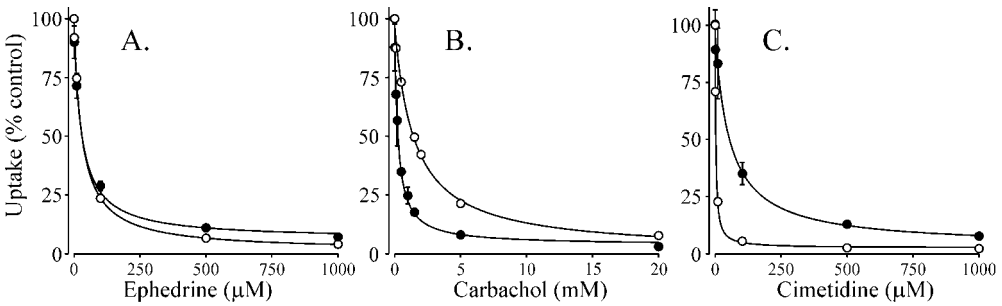

Fig. 4. Relative effect on increasing concentrations of ephedrine (A), carbachol (B), or cimetidine (C) on uptake of [^{14}C]TEA mediated by either hOCT2 (●) or rbOCT2 (○). Each point is mean (±S.E.) of uptakes measured under each condition measured in two separate experiments. Data were normalized to the level of uptake measured in the absence of the test inhibitor. Lines were fit to the data using a nonlinear regression algorithm (SigmaPlot 3.0). IC_{50} values are listed in Table 1.

confidence ($r^2 = 0.49 \pm 0.09$) that represents 4.25 standard deviations from the original model described in eq. 4. It is interesting that Cerius^2 was, however, unable to converge on a model describing binding of the training set molecules to rbOCT2 using these same descriptors.

The model outlined in eq. 4 was used to predict, for hOCT2, the IC_{50} values for a test set of six diverse compounds selected to reflect the structural diversity associated with the training set. Although the predicted IC_{50} of one of the six test compounds (ibuprofen) was poorly predicted (Fig. 8A, open circles), predicted versus measured IC_{50} values for the remaining five compounds resulted in an $r^2 = 0.68$.

Inhibition Studies with N^1-Substituted Pyridiniums and Quinoliniums with hOCT2. A set of N^1-substituted pyridiniums containing a phenyl substituent at the 3- or 4-position was investigated to determine whether the 3D placement of this hydrophobic mass influenced binding to hOCT2. The N^1 substituent was also varied to increase the compound's hydrophobicity (hydroxyl ethyl < ethyl < benzyl). Table 2 shows the ALogP and IC_{50} values generated for each compound. The data show that as the hydrophobic phenyl ring is rotated about the pyridinium, there is no change in affinity for the transporter. However, as hydrophobicity of the N^1 substituent was increased, the affinity for the transporter was also increased. In addition, a set of quinoliniums, also containing the differing N^1 substituents mentioned above, were tested. Again, affinity was positively correlated with hydrophobicity, and IC_{50} values were very similar to those for the corresponding 3- or 4-phenylpyridinium. The correlation between log IC_{50} and AlogP and CLogP for these nine compounds was $r^2 = 0.85$ and 0.57, respectively, whereas the Cerius^2 2D-QSAR predicted these same molecules with $r^2 = 0.70$. In a previous study (Bednarczyk et al., 2003), these two sets of compounds were used to perform inhibition kinetics of TEA in HeLa cells stably transfected with hOCT1; IC_{50} values generated in this study are listed in Table 2. As with hOCT2, a decrease in the IC_{50} values for interaction with hOCT1 was correlated with an increase in hydrophobicity for all subsets of compounds. However, unlike the situation observed for hOCT2, as the hydrophobic mass was rotated around the pyridinium, IC_{50} for interaction with hOCT1 increased, suggesting spatial arrangement of hydrophobic mass effects a compound's interaction with hOCT1 more substantially than with hOCT2.

When all the test set molecules were combined with the training set, a total of 45 molecules were available for model building. Using stepwise regression the r^2 decreased to 0.70, $q^2 = 0.55$, F-test = 18.4.

$$\text{Log } IC_{50} = 3.07539 + 0.202466 \times \text{Rotatable bonds} - 0.306335 \times \text{AlogP98} - 0.00051953 \times \text{JURS-DPSA-2} - 0.0037616 \times \text{Jurs-TASA} + 0.168926 \text{ CLogP} \quad (5)$$

The model was randomized nine times to give 90% confidence with $r^2 = 0.42 \pm 0.10$, which represents 4.07 standard deviations from the original model eq. 4. It would seem that adding these data caused deterioration in the model statistics, probably because of the inclusion of the phenylpyridinium compounds for which hydrophobicity seems to be disproportionately important for binding. The importance of

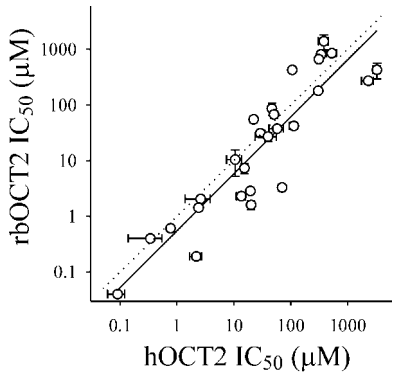

Fig. 5. Comparison of IC_{50} values for inhibition of [^{14}C]TEA transport mediated by hOCT2 (*x*-axis) or rbOCT2 (*y*-axis). Each point is the mean of two or three IC_{50} values measured in cells expressing either the human or rabbit ortholog of OCT2 (±S.E.). The solid line is the linear regression of the logs of the measured and calculated parameters; the dotted line is the line of unity.

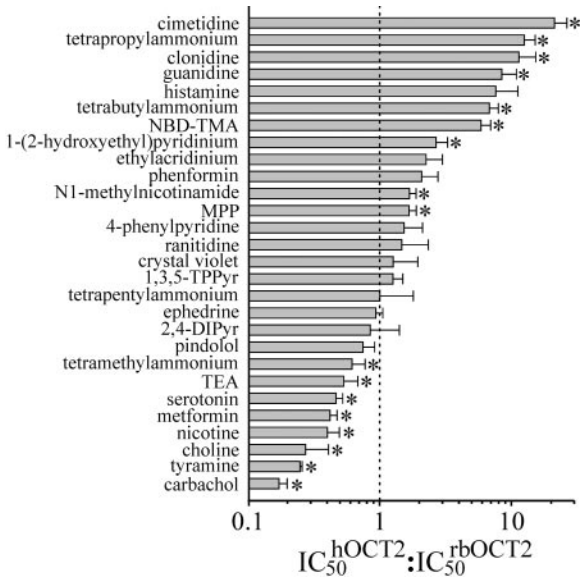

Fig. 6. Comparison of the relative effect of each test compound as an inhibitor of hOCT2 versus rbOCT2. The length of each bar represents the ratio of a test agent's IC_{50} for inhibition of TEA transport mediated by hOCT2, to that for transport mediated by rbOCT2. Error bars reflect the sum of the SEs determined for each agent as an inhibitor of the human and rabbit transporters. Asterisks designate those ratios that differed from unity by more than two times the sum of the individual SEs.

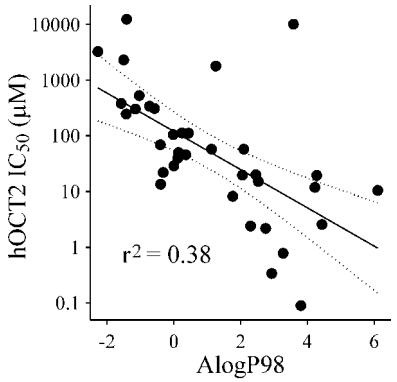

Fig. 7. Relationship between the IC_{50} for inhibition of TEA transport mediated by hOCT2 and that compound's calculated oil/water partition coefficient (expressed as ALogP98, determined by Cerius^2). The solid line is the regression of these two parameters; the dotted lines indicate 95% confidence limits.

hydrophobicity is evident in the inclusion of AlogP, CLogP, and the Jurs descriptors (total hydrophobic surface area; DPSA-2, difference in total charge weighted surface areas). Figure 8B shows the relationship between the experimentally determined IC_{50} values for the 45 test compounds and the values predicted using eq. 5. Exclusion of three anionic compounds (*para*-aminohippurate, probenecid, and ibuprofen; open diamonds) increased the correlation between measured and predicted ($r^2 = 0.81$).

3D-QSAR (CoMFA). A FieldFit alignment based on manually selected overlapping points was used as a basis to generate CoMFA models for human and rabbit OCT2. Both transporters displayed the greatest apparent affinity for ethylacridinium (IC_{50} values of 90 and 40 nM for hOCT2 and rbOCT2, respectively; Table 1), so it was selected as the template molecule for overlapping all other OCs. The positively charged nitronium and the center of hydrophobic mass were used as two features to guide the alignment. A force constant of 20 was used for FieldFit. All aligned structures were relaxed and then submitted to CoMFA analysis. Test set compounds (clonidine, guanidine, tetramethylammonium, N^1-hydroxyethylpyridinium, and 2,4-dimethyl-9-*H*-indenol1[2,1-*c*]pyridinium) were randomly selected while maintaining the coverage of training set activity. The following fields were generated for each CoMFA model: CoMFA_standard; CoMFA_indicator; CoMFA_parabolic; CoMFA_Hbond; CLogP; and Molconn-Z. The correlation between each of these descriptor fields and measured IC_{50} values was calculated and compared. Pindolol and ibuprofen were identified as outliers both by Factor Analysis and CoMFA runs and so were excluded from both CoMFA models. The QSAR statistics for the best correlation are listed in Table 3.

CoMFA contours at 80% confidence levels were generated for each model, and these are shown in Fig. 9. A large blue contour covering the positive center (mainly ammonium) suggests an important role for positive charge at this position. The small green contour over the phenol ring indicates the necessity of a sterically bulky group at this position. These two features should be expected because of the way our alignment was set up. It is interesting that a red contour next to the green contour showed up in both human and rabbit CoMFA models. This suggests a correlation between electronegative charge in this area and higher affinity to OCT2. Furthermore, this could indicate that a small negative charge or delocalized point charge close to the positive center might play a stabilizing role in the binding of substrates to OCT2. Figure 10 shows the relationship between predicted versus measured log IC_{50} values for the training and test sets for human and rabbit OCT2. The predictive value of the CoMFA models is evident in the r^2 values of 0.97 for both training sets, and r^2 values of 0.85 to 0.89 for the test set for human and rabbit OCT2, respectively. It should be noted that both models had difficulty predicting 2,4-dimethyl-9-*H*-

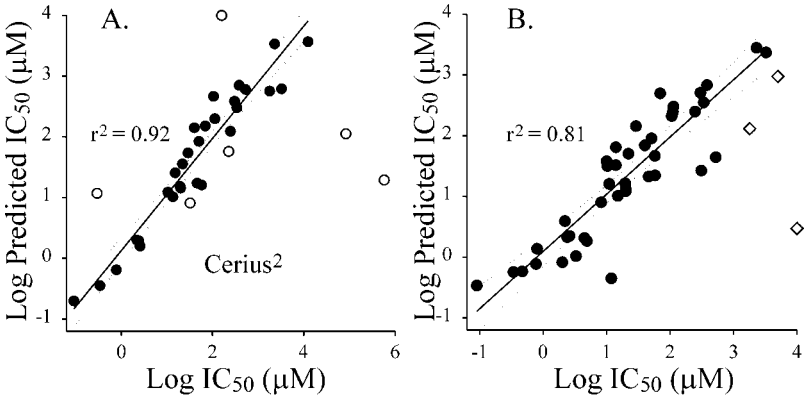

Fig. 8. A, relationship for hOCT2 between the IC_{50} values predicted using the 2D-QSAR (Cerius^2) outlined in eq. 4 (see text) and the measured IC_{50} values for the training set of 30 compounds (●) and the test set of six compounds (○). The solid line represents the regression of predicted versus measured IC_{50} for the training set ($r^2 = 0.92$). The major outliers of the test set (from left to right) were 3,5-dimethyl-4-phenylpyridine-1-oxide, ibuprofen, famotidine, and amantidine. B, relationship between the IC_{50} values using the 2D-QSAR (Cerius^2) outlined in eq. 5 (see text) and the measured IC_{50} values for the complete set of cationic compounds employed in this study [45 molecules (●)]. The three anionic compounds studied [PAH, probenecid, and ibuprofen (◇)] were excluded from the analysis as they represent outliers. The solid line represents the regression of predicted versus measured IC_{50} for the training set ($r^2 = 0.81$; dotted lines represent 95% confidence limits).

TABLE 2

IC_{50} values for the inhibition of TEA by the phenylpyridiniums and quinoliniums in CHO cells stably transfected with hOCT2 (this study) and HeLa cells stably transfected with hOCT1 (Bednarczyk et al., 2003)

Each IC_{50} is the mean value of at least two experiments (described under *Materials and Methods*). ClogP values calculated with Daylight software using Cerius^2 (Accelrys).

Compound	IC_{50}		AlogP
	hOCT2	hOCT1	
	μM		
1-(2-Hydroxyethyl)-4-phenylpyridinium	10.3 ± 1.9	16.2 ± 1.4	1.76
1-(2-Hydroxyethyl)-3-phenylpyridinium	10 ± 2.3	31.1 ± 2.3	1.76
1-(2-Hydroxyethyl)quinolinium	14 ± 0.9	80.6 ± 3.2	1.58
1-(Phenyl)methyl-4-phenylpyridinium	2 ± 0.1	9.3 ± 0.6	3.88
1-(Phenyl)methyl-3-phenylpyridinium	0.8 ± 0.1	5.5 ± 0.9	3.88
1-(Phenyl)methylquinolinium	0.47 ± 0.06	14.3 ± 0.7	3.70
1-Ethyl-4-phenylpyridinium	4.9 ± 0.8	7.1 ± 1.1	2.65
1-Ethyl-3-phenylpyridinium	4.45 ± 0.7	28.3 ± 4.5	2.65
1-Ethylquinolinium	3.3 ± 0.5	67.6 ± 11.2	2.47

indenol[2,1-*c*]pyridinium (residual values 3.73 and 5.63 μM for hOCT2 and rbOCT2, respectively), most likely caused by a slight misaligned overlap of its nitrogen group out of plane from the position where the other molecules' electropositive moieties reside (data not shown).

OCT2 HipHop pharmacophore Development. The common feature alignment of four selective rbOCT2 inhibitors suggested a pharmacophore that was characterized by a positive charge feature and a hydrogen bond donor at a distance of 5.89 Å with an angle of 129.97° between the positive charge and the hydrogen bond donor vector (Fig. 11A shows alignment of cimetidine within the pharmacophore). Ephedrine was used as an example of a molecule with no disproportionate selectivity for either transporter; it shows intermediate mapping to both pharmacophores (Fig. 11, B and C). The alignment of the six most selective hOCT2 inhibitors suggested a pharmacophore with a positive charge feature and a hydrogen bond acceptor feature at a distance of 5.72 Å with an angle of 92.76° between the positive charge and the hydrogen bond acceptor vector (Fig. 11D shows alignment of carbachol within the pharmacophore).

Discussion

In light of the increasing pharmacological significance of renal secretion as a defining factor in the bioavailability of a vast array of cationic drugs (Balant and Gex-Fabry, 1990; Chaturvedi et al., 2001), there is obvious value to the ability to predict the extent to which potential substrates interact with key elements in the renal secretory pathway. Ullrich made a detailed study of the structural specificity of basolateral organic cation transport in rat kidney using the in vivo stopped-flow capillary microperfusion technique (Ullrich et al., 1991, 1992). Interpretation of their observations is complicated by the current knowledge that, in rat kidney, basolateral OC transport involves at least two transporters, i.e., OCT1 and OCT2, which have, for at least some substrates, very different selectivity characteristics (Arndt et al., 2001; Urakami et al., 2001). Therefore, the general rules concerning the physicochemical factors that influence substrate binding to OCTs must be viewed as an average response of the interaction with multiple transporters operating in parallel. Nevertheless, the principal factor influencing substrate interaction with OCTs was found to be hydrophobicity, in concurrence with some of the earliest studies on renal OC secretion (Green et al., 1959). In the present study, there was a correlation, albeit weak ($r^2 = 0.38$), between hydrophobicity and the interaction of our training set with hOCT2. A similar observation was noted in a recent examination of the factors that influence substrate binding to hOCT1 (Bednarczyk et al., 2003). Although within a group of structurally related compounds binding efficacy can be more closely correlated with hydrophobicity as a single criterion for interaction with OCTs (Zhang et al., 1999; Dresser et al., 2002), it is evident, and not surprising, that factors other than the oil/water

TABLE 3
CoMFA statistics for human and rabbit OCT2 models

	PRESS	Q Square	No. of Components	r Square	s	% Steric	% Electrostatic
hOCT2	0.71	0.596	4	0.973	0.182	0.65	0.35
rbOCT2	0.918	0.531	4	0.972	0.224	0.65	0.35

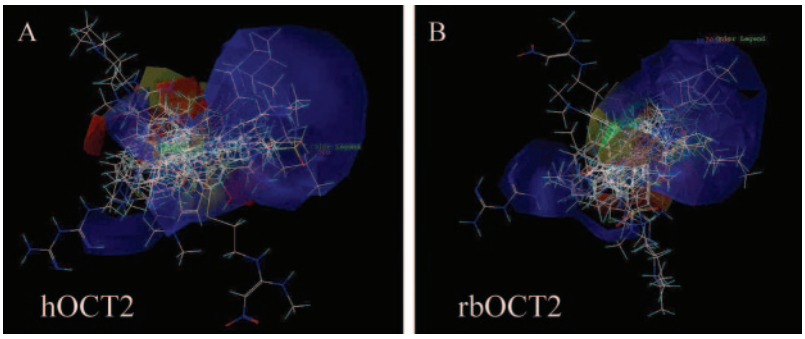

Fig. 9. Structural overlap of the OCT2 compounds used in this study and CoMFA contour maps for hOCT2 ($q^2 = 0.60$) (A) and rbOCT2 ($q^2 = 0.53$) (B). Red and blue contours are visualized at the 20% standard coefficient level, representing those areas surrounding the molecules where electronegative and positive charge, respectively, significantly contribute to OCT2 IC_{50} values. Likewise, green and yellow contours indicate the fields where steric bulk significantly increases or decreases OCT2 IC_{50} values, respectively.

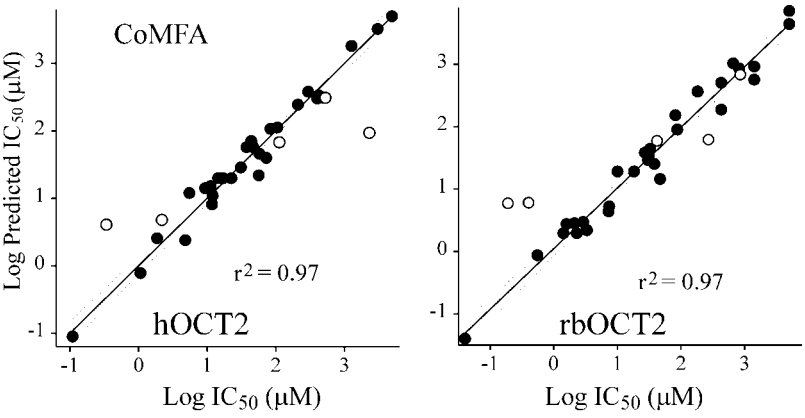

Fig. 10. Relationship between predicted and measured hOCT2 (A) and rbOCT2 (B) IC_{50} values for the complete set of cationic compounds used in this study (training set, ●; test set, ○). The solid line represents the regression of predicted versus measured IC_{50} for the training set ($r^2 = 0.97$; dotted lines represent 95% confidence limits). For hOCT2 the leftmost test set outlier was 2,4-dimethyl-9-*H*-indenol[2,1-*c*]pyridinium; the right most outlier was guanidine. For rbOCT2, the leftmost outliers were clonidine and 2,4-dimethyl-9-*H*-indenol[2,1-*c*]pyridinium.

partition coefficient (or predictors of this property) play key roles in stabilizing substrate binding to OCTs.

The present study is, to the best of our knowledge, the first to apply a combination of in vitro and computational approaches to identify factors other than hydrophobicity that play a role in defining substrate interactions with OCT2. Our effort to develop a strategy for predicting molecular criteria that influence binding to OCT2 involved the use of two different computational methods, namely, Cerius^2 to develop a 2D-QSAR model of substrate interaction and CoMFA to develop a 3D-QSAR model. The latter, in addition to predicting binding efficacy also held the promise of providing visual information on the structural determinants that influence substrate-transporter interaction. The Cerius^2 models (eqs. 4 and 5) did underscore the importance of hydrophobicity as a determinant in influencing substrate binding to hOCT2, as they were dominated by parameters such as AlogP98, CLogP, and Jurs descriptors. However, a role for steric factors was also suggested in eq. 4 by the inclusion of a Shadow parameter (Shadow YZ; area of the molecular shadow in the YZ plane). It is interesting that our previous study on characteristics of binding hOCT1 identified Shadow nu (ratio of largest to smallest dimension) as a principal determinant of substrate interaction for this transporter (Bednarczyk et al., 2003). In the previous study, we noted that the placement of planar hydrophobic mass about a pyridinium nucleus exerted a systematic effect on binding to hOCT1 (i.e., 4-phenylpyridinium compounds interacted with substantially lower IC_{50} values than did, for example, quinolinium compounds), consistent with the conclusion that the hOCT1 binding sites favors binding of "longer", rather that "wider," molecules. In contrast, in the present study, we found no such systematic effect with respect to the binding of 4-phenyl-, 3-phenyl versus quinolinium compounds (Table 2), and this was reflected in emphasis on binding of a bulk area term (Shadow YZ) rather than a term that emphasized the binding efficacy of long, narrow substrates. The presence of the rotatable bond descriptor suggests that hOCT2 may also prefer flexible substrates, a characteristic not implicated in hOCT1 binding. The degree of substrate ionization indicated as important for hOCT2 substrate binding was not evaluated in these computational studies (Barendt and Wright, 2002). It should also be noted that both the 2D and 3D analyses used here implicitly assume that the binding site/region of OCT2 has similar characteristics when exposed to extracellular and cytoplasmic aspects of the membrane and, for at least some substrates (e.g., tetrabutylammonium and corticosterone) this has been shown not to be the case (Volk et al., 2003). Therefore, the models describe a hypothetical binding site with mixed properties of the extracellular and intracellular oriented conformations of the transporter.

The 3D-QSAR that resulted from application of CoMFA served to emphasize two important issues concerning the influence of molecular size/shape on binding of substrate to OCTs. First, it underscored the observation, suggested by the 2D-QSAR, that steric factors clearly play a role in the binding process. This is evident in the marked improvement in predictive power of the 3D-QSAR (r^2 = 0.97; Fig. 10) compared with the 2D-QSAR (r^2 = 0.8–0.9; Fig. 8). The second issue evident from the CoMFA, interestingly, was the multispecificity of the binding site evident from the substrate overlays within the binding region (Fig. 9). Although the CoMFA contour plot indicates that binding is enhanced or reduced by, for example, the presence of steric mass in particular positions (i.e., green versus yellow contours, respectively), it is also evident that the OCT2 binding site (both for human and rabbit) is extremely permissive with respect to the presence and placement of, in particular, hydrophobic moieties that radiate away from a positively charged binding center. The capacity to interact effectively with such a structurally diverse set of compounds has important implications for the structural nature of the OCT2 binding site. This clearly represents a challenge for future efforts to model the binding site by identifying structural features that permit comparatively high-affinity interactions with molecules as structurally diverse as, for example, MPP (IC_{50} = 2.4 μM) and crystal violet (IC_{50} = 2.6 μM) (Table 1).

Comparison of the selectivity of the human and rabbit orthologs of OCT2 is also instructive. Whereas the two orthologs displayed very similar apparent affinities for many of the test agents, it was also evident that for just as many compounds their selectivities differed substantially (Fig. 5). It is noteworthy that these differences were not systematic: for some compounds, e.g., carbachol and tyramine, hOCT2 displayed a 5–15-fold higher affinity, whereas for other compounds, e.g., cimetidine and clonidine, it was the rabbit ortholog that displayed a higher (5–10-fold) affinity (Fig. 6). The primary sequences of human and rabbit OCT2 are 96% similar (83% identical). The differences in selectivity between these two transporters presumably reflect structural differences, probably minor ones, the consequences of which include clearly distinct selectivity profiles. Although this is not a surprising observation, it serves to emphasize that minor changes in a few amino acid residues can result in very significant changes in selectivity for some substrates, whereas having no effect on interaction with other substrates. For example, Gorboulev et al. (1999) found that substituting a glutamate residue for the aspartate found at

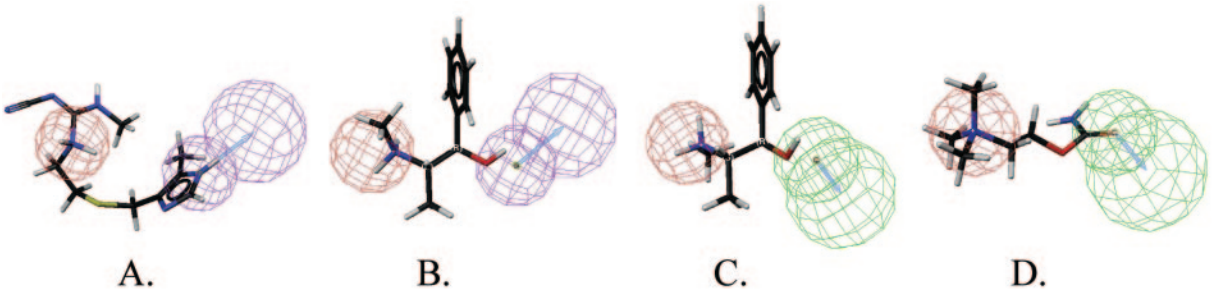

Fig. 11. HipHop pharmacophores for rbOCT2 and hOCT2. A, cimetidine mapped to rabbit HipHop model. B, ephedrine mapped to rabbit HipHop model. C, ephedrine mapped to human HipHop model. D, carbachol mapped to human HipHop model.

position 475 in rat OCT1 resulted in an 8-fold increase in apparent affinity for TEA but that it had no effect on the interaction of the transporter with MPP. Likewise, Leabman et al. (2002) noted that single nucleotide polymorphisms (SNPs) in hOCT2 exerted substrate-specific effects on transport function. For example, the K432Q SNP increased apparent affinity of the transporter for tetrabutylammonium and MPP, whereas having little or no effect on interaction of the transporter for metformin and quinidine. On the other hand, the A270S SNP decreased apparent affinity for MPP and tetrabutylammonium, whereas having no significant effect on interaction with metformin and quinidine. The differences in selectivity between the human and rabbit OCT2 also emphasize the care that must be used when extending to humans observations obtained in studies using nonhuman orthologs.

Knowing that there are molecules that discriminate between the human and rabbit orthologs of OCT2 provided an opportunity to probe the qualitative differences between molecules with high affinity to the hOCT2 and rbOCT2 transporters using a Catalyst HipHop alignment. An alignment of the selective inhibitors for both transporters indicated subtle but distinctive differences for recognition, which manifested in differences in features and angles recognized for each transporter (Fig. 11, A–D). The assessment of ephedrine, which shows no selectivity for either transporter, indicates that this molecule can adequately map to both pharmacophores (Fig. 11, B and C). This pharmacophore analysis provides valuable information that can be used for testing subsequent homology models for both transporters by comparing the pharmacophores and aligned selective inhibitors docked into the transporters. Even though the features on these pharmacophores are similar, the approach is sensitive enough to identify a difference in the orientation of the hydrogen bonding features (>37°). This could infer variability in the disposition of critical amino acids for interaction with inhibitors within the respective transporters.

In summary, computationally derived QSAR models of the basis of OCT2 selectivity were determined for the human and rabbit orthologs of the renal organic cation transporter, OCT2. A 2D-QSAR emphasized the importance of hydrophobicity as an important determinant in the binding of substrates to OCT2 alongside structural bulk and molecular flexibility. A 3D-QSAR displayed better predictive power and served to emphasize the fact that molecular size and shape plays a significant role in defining the interaction of substrates. The CoMFA models also highlighted the multispecificity of the OCT2 binding site by noting the importance of structural features in selected regions, and the permissiveness of the binding site with respect to steric bulk in other regions. Marked differences in the selectivity of the human and rabbit orthologs of OCT2 also underscored the fact that very modest differences in the amino acid residue composition of the protein can result in substantial changes in affinity of the respective transporters for some substrates, whereas having no effect on the interaction with other substrates. The general hydrophobic substrate promiscuity of the OCT2 transporter draws immediate parallels with P-glycoprotein and other proteins of importance to drug discovery that can bind a diverse array of xenobiotics to ultimately aid in their elimination from the body (Ekins, 2004).

References

Arndt P, Volk C, Gorboulev V, Budiman T, Popp C, Ulzheimer-Teuber I, Akhoundova A, Koppatz S, Bamberg E, Nagel G, et al. (2001) Interaction of cations, anions and weak base quinine with rat renal cation transporter rOCT2 compared with rOCT1. *Am J Physiol* **281:**F454–F468.

Balant LP and Gex-Fabry M (1990) Physiological pharmacokinetic modelling. *Xenobiotica* **20:**1241–1257.

Barendt WM and Wright SH (2002) The human organic cation transporter (hOCT2) recognizes the degree of substrate ionization. *J Biol Chem* **277:**22491–22496.

Bednarczyk D, Ekins S, Wikel JH, and Wright SH (2003) Influence of molecular structure on substrate binding to the human organic cation transporter, hOCT1. *Mol Pharmacol* **63:**489–498.

Bednarczyk D, Mash EA, Aavula BR, and Wright SH (2000) NBD-TMA: a novel fluorescent substrate of the peritubular organic cation transporter of renal proximal tubules. *Pflueg Arch Eur J Physiol* **440:**184–192.

Busch AE, Karbach U, Miska D, Gorboulev V, Akhoundova A, Volk C, Arndt P, Ulzheimer JC, Sonders MS, Baumann C, et al. (1998) Human neurons express the polyspecific cation transporter hOCT2, which translocates monoamine neurotransmitters, amantadine and memantine. *Mol Pharmacol* **54:**342–352.

Chaturvedi PR, Decker CJ, and Odinecs A (2001) Prediction of pharmacokinetic properties using experimental approaches during early drug discovery. *Curr Opin Chem Biol* **5:**452–463.

Clement OO and Mehl AT (2000) HipHop: pharmacophore based on multiple common-feature alignments, in *Pharmacophore Perception, Development and Use in Drug Design* (Guner OF ed) pp 69–84, IUL, San Diego.

Dresser MJ, Xiao G, Leabman MK, Gray AT, and Giacomini KM (2002) Interactions of n-tetraalkylammonium compounds and biguanides with a human renal organic cation transporter (hOCT2). *Pharm Res* **19:**1244–1247.

Ekins S (2004) Predicting undesirable drug interactions with promiscuous proteins in silico. *Drug Discov Today* **9:**276–285.

Gorboulev V, Volk C, Arndt P, Akhoundova A, and Koepsell H (1999) Selectivity of the polyspecific cation transporter rOCT1 is changed by mutation of aspartate 475 to glutamate. *Mol Pharmacol* **56:**1254–1261.

Green RE, Ricker WE, Attwood WL, Koh YS, and Peters L (1959) Studies of the renal tubular transport characteristics of N^1-methylnicotinamide and tetraalkylammonium compounds in the avian kidney. *J Pharmacol Exp Ther* **126:**195–201.

Groves CE, Evans K, Dantzler WH, and Wright SH (1994) Peritubular organic cation transport in isolated rabbit proximal tubules. *Am J Physiol* **266:**F450–F458.

Jonker JW and Schinkel AH (2004) Pharmacological and physiological functions of the polyspecific organic cation transporters: OCT1, 2 and 3 (SLC22A1–3). *J Pharmacol Exp Ther* **308:**2–9.

Jonker JW, Wagenaar E, Van Eijl S, and Schinkel AH (2003) Deficiency in the organic cation transporters 1 and 2 (Oct1/Oct2 [Slc22a1/Slc22a2]) in mice abolishes renal secretion of organic cations. *Mol Cell Biol* **23:**7902–7908.

Kaewmokul S, Chatsudthipong V, Evans KK, Dantzler WH, and Wright SH (2003) Functional mapping of rbOCT1 and rbOCT2 activity in the S2 segment of rabbit proximal tubule. *Am J Physiol* **285:**F1149–F1159.

Karbach U, Kricke J, Meyer-Wentrup F, Gorboulev V, Volk C, Loffing-Cueni D, Kaissling B, Bachmann S, and Koepsell H (2000) Localization of organic cation transporters OCT1 and OCT2 in rat kidney. *Am J Physiol* **279:**F679–F687.

Koepsell H (2004) Polyspecific organic cation transporters: their functions and interactions with drugs. *Trends Pharmacol Sci* **25:**375–381.

Koepsell H and Endou H (2004) The SLC22 drug transporter family. *Pflueg Arch Eur J Physiol* **447:**666–676.

Koepsell H, Schmitt BM, and Gorboulev V (2003) Organic cation transporters. *Rev Physiol Biochem Pharmacol* **150:**36–90.

Leabman MK, Huang CC, Kawamoto M, Johns SJ, Stryke D, Ferrin TE, DeYoung J, Taylor T, Clark AG, Herskowitz I, et al. (2002) Polymorphisms in a human kidney xenobiotic transporter, OCT2, exhibit altered function. *Pharmacogenetics* **12:**395–405.

Malo C and Berteloot A (1991) Analysis of kinetic data in transport studies: new insights from kinetic studies of Na^+-D-glucose cotransport in human intestinal brush-border membrane vesicles using a fast sampling, rapid filtration apparatus. *J Membr Biol* **122:**127–141.

Meijer DKF, Mol WEM, Müller M, and Kurz G (1990) Carrier-mediated transport in the hepatic distribution and elimination of drugs, with special reference to the category of organic cations. *J Pharmacokin Biopharmaceut* **18:**35–70.

Motohashi H, Sakurai Y, Saito H, Masuda S, Urakami Y, Goto M, Fukatsu A, Ogawa O, and Inui K-I (2002) Gene expression levels and immunolocalization of organic anion transporters in the human kidney. *J Am Soc Nephrol* **13:**866–874.

Ullrich KJ (1999) Affinity of drugs to the different renal transporters for organic anions and organic cations. *Pharm Biotechnol* **12:**159–179.

Ullrich KJ, Papavassiliou F, David C, Rumrich G, and Fritzsch G (1991) Contraluminal transport of organic cations in the proximal tubule of the rat kidney. I. Kinetics of N^1-methylnicotinamide and tetraethylammonium, influence of K^+, HCO_3, pH; inhibition by aliphatic primary, secondary and tertiary amines and mono- and bisquaternary compounds. *Pflueg Arch Eur J Physiol* **419:**84–92.

Ullrich KJ, Rumrich G, and Fritzsch G (1992) Contraluminal transport of organic cations in the proximal tubule of the rat kidney. II. Specificity: anilines, phenylalkylamines (catecholamines), heterocyclic compounds (pyridines, quinolines, acridines). *Pflueg Arch Eur J Physiol* **420:**29–38.

Urakami Y, Okuda M, Masuda S, Akazawa M, Saito H, and Inui K (2001) Distinct characteristics of organic cation transporters, OCT1 and OCT2, in the basolateral membrane of renal tubules. *Pharm Res* **18:**1528–1534.

van Montfoort JE, Muller M, Groothuis GM, Meijer DK, Koepsell H, and Meier PJ (2001) Comparison of "type I" and "type II" organic cation transport by organic cation transporters and organic anion-transporting polypeptides. *J Pharmacol Exp Ther* **298:**110–115.

Volk C, Gorboulev V, Budiman T, Nagel G, and Koepsell H (2003) Different affinities

of inhibitors to the outwardly and inwardly directed substrate binding site of organic cation transporter 2. *Mol Pharmacol* **64:**1037–1047.
Wright SH and Dantzler WH (2004) Molecular and cellular physiology of renal organic cation and anion transport. *Physiol Rev* **84:**987–1049.
Wright SH and Wunz TM (1999) Influence of substrate structure on substrate binding to the renal organic cation/H^+ exchanger. *Pflueg Arch Eur J Physiol* **437:**603–610.
Wright SH, Wunz TM, and Wunz TP (1995) Structure and interaction of inhibitors with the TEA/H^+ exchanger of rabbit renal brush border membranes. *Pflueg Arch Eur J Physiol* **429:**313–324.
Zhang L, Gorset W, Dresser MJ, and Giacomini KM (1999) The interaction of n-tetraalkylammonium compounds with a human organic cation transporter, hOCT1. *J Pharmacol Exp Ther* **288:**1192–1198.
Zhang X, Evans KK, and Wright SH (2003) Molecular cloning of rabbit organic cation transporter rbOCT2 and functional comparisons with rbOCT1. *Am J Physiol* **283:**F124–F133.

Address correspondence to: Dr. Stephen H. Wright, Department of Physiology, College of Medicine, University of Arizona, Tucson, AZ 85724. E-mail: shwright@u.arizona.edu